https://doi.org/10.48048/tis.2024.7320

Decreasing of Magnetic Saturation of Yttrium Doped Cobalt Ferrite Prepared by the Sol-Gel Auto-Combustion

Dwi Teguh Rahardjo[1,2,*], Sri Budiawanti[2], Suharno Suharno[2], Risa Suryana[1], Agus Supriyanto[1] and Budi Purnama[1]

[1]Department of Physics, Faculty of Mathematics and Natural Sciences, Universitas Sebelas Maret, Surakarta 57126, Indonesia
[2]Department of Physics Education, Faculty of Teacher Training and Education, Universitas Sebelas Maret, Surakarta 57126, Indonesia

([*]Corresponding author's e-mail: dwiteguh@staff.uns.ac.id)

Received: 14 July 2023, Revised: 9 August 2023, Accepted: 18 August 2023, Published: 1 February 2024

Abstract

In this research, a nano-sized cobalt ferrite material doped with Yttrium has been successfully fabricated using the sol-gel method of automatic combustion with variations in low sintering temperatures of 200, 300 and 400 °C. The results of refinement of XRD data using the Rietveld method show that the Yttrium-doped cobalt ferrite compound with a Yttrium concentration molarity of 0.1 possess a cubic crystal system and Fd-3m space group. The increasing annealing temperatures also increase the crystallite size of Yttrium-doped cobalt ferrite with the highest magnitude of 16.05 nm. The FTIR results of the samples indicated the presence of Co-O bonds around wave number 385 cm^{-1} and Fe-O bonds around wave number 582 cm^{-1} which are characteristic of the presence of cobalt ferrite compounds. From the VSM measurement results, it can be seen that there is a decrease in magnetic saturation with an increase in annealing temperature. The presence of Yttrium substitution, which takes the place of Fe^{3+} in cobalt ferrite material, indicates lower saturation magnetization. Image from SEM results showed samples have nanoparticle crystallite size. Evaluation of potential photocatalyst applications using a UV-Visible Spectrophotometer (UV-Vis). For Yttrium doped cobalt ferrite at 200 °C, the best degradation efficiency of Congo Red findings showed a magnitude of 76.10 %; the results are confirmed by the occurrence of the smallest crystallite size (15.11 nm).

Keywords: Sol-gel auto-combustion, Yttrium-doped, Cobalt ferrite, Annealing, Saturation magnetization, Photocatalytic, Congo red

Introduction

Researchers in several countries have studied cobalt ferrite magnetic material over the last few decades. Cobalt ferrite magnetic material has many applications in various fields of human life. Some of the magnetic properties possessed by cobalt ferrite magnetic materials can have useful applications in many fields, namely energy, transformers [1], sensors [2,3], microwave shielding [4,5], supercapacitor [6], drug delivery [7,8], and catalysis [9,10]. The variation of the annealing temperature of cobalt ferrite magnetic material preparation could affect the crystallite size of the cobalt ferrite [11]. Substituting rare earth elements in cobalt ferrite magnetic materials can increase optical and magnetic properties [12]. Modifying cobalt ferrite nanoparticle-based materials through rare earth metal substitution can affect dye absorption [13]. The rare earth of cerium-substituted cobalt ferrite influences nanocrystalline cobalt ferrite structure and magnetic properties [14]. Meanwhile, replacing which rare earth element with Erbium can affect the dielectric and electrical conductivity of cobalt ferrite compounds [15]. Doping of rare earth elements Gadolinium and Samarium can affect the microstructural properties of cobalt ferrite compounds [16]. Cobalt ferrite doped with rare earth Cerium can improve electrical transport by applying a thin resistive layer to the temporary data storage for magnetic recording devices [17]. Cobalt ferrite compounds doped with rare earth elements can also enhance catalytic properties [18].

Several papers were reported from previous research with yttrium rare-earth elements as doping in cobalt ferrite nanoparticles. Variations in the molarity concentration of yttrium elements in cobalt ferrite compounds can affect structural, magnetic, and optic properties [19]. The increasing molarity concentration of yttrium-doped cobalt ferrite can decrease lattice strain and the length of the lattice constant [20], reduce magnetic saturation [20,21], and decrease crystallite size [21-23]. The decreasing molarity concentration of

yttrium-doped cobalt ferrite can also increase the energy band gap of cobalt ferrite compounds [24] and dielectric permittivity [25]. Various methods can prepare yttrium-doped cobalt ferrite nanoparticle samples. The main methods of preparing the cobalt ferrite nanoparticles through wet procedures are sol-gel auto combustion [26], coprecipitation [27,28], and hydrothermal, which result in comparative physical parameters of structure, magnetic, and optic properties. The increasing sintering temperature on synthesis of yttrium doped cobalt ferrite compound affects the increase in crystallite size [29], decrease lattice constant, and lattice strain [30]. In addition, the clout of increasing the low sintering temperature on the magnetic properties of yttrium-doped cobalt ferrite has yet to be widely reported.

Therefore, this paper presents the synthesis of yttrium-doped cobalt ferrite produced using the sol-gel auto-combustion procedure with low sintering temperature variations, 200, 300 and 400 °C. The sol-gel auto-combustion method was chosen because of its low cost, low crystallinity formation temperature, and simple synthesis procedure [31]. The crystalline structure, magnetic properties, and optic properties of yttrium-doped cobalt ferrite nanoparticles were analyzed using XRD, FTIR, VSM, SEM, and UV-Vis.

Materials and methods

Materials

The chemical compounds used to synthesize yttrium doped cobalt ferrite $CoY_{0.1}Fe_{1.9}O_4$ were Ferrite (III) nitrate nonahydrate $Fe(NO_3)_3.9H_2O$, Cobalt (II) nitrate hexahydrate $Co(NO_3)_2.6H_2O$, Yttrium (III) nitrate hexahydrate $Y(NO_3)_3.6H_2O$, and Citric acid $C_6H_8O_7.H_2O$. All chemical compounds in this research were purchased from Merck and directly used without special treatment.

Methods and measurements

The $CoY_{0.1}Fe_{1.9}O_4$ nanopowder was synthesized with the sol-gel auto combustion. The addition of $C_6H_8O_7.H_2O$ compounds is used as an automatic burner. The molarity ratio of $Co(NO_3)_2.6H_2O$, $Y(NO_3)_3.6H_2O$, and $Fe(NO_3)_3.9H_2O$ is 9:1:20. The solution was stirred for approximately 3 h at 90 °C until the gel product was obtained. The gel was dried at 150 °C for 2 h under atmospheric conditions to get a brownish-black product. After that, the obtained product is then crushed with a mortar manually and sintered at temperatures of 200, 300 and 400 °C, for 4 h. The products were characterized using an X-Ray Diffractometer (XRD) from PanAnalytical, Type: E'xpert Pro with Cu Kα1 radiation source of 1.54056 Å, for identifying the emergence of functional groups of samples were shown using Fourier Transform Infra-Red (FTIR) spectroscopy from Shimadzu IR Prestige 21, samples magnetic properties were shown using Vibrating Sample Magnetometer (VSM) from Oxford type VSM 1.2H, samples surface profile were shown using Scanning Electron Microscopy (SEM), and the content of the elements is indicated using Energy Dispersive X-ray (EDX) type of Inspect-S50. Finally, the photocatalytic procedure of Congo red dye was irradiated using a UV light source for 30 min. The photocatalytic evaluation was performed using a UV-Visible Spectrophotometer (UV-Vis Spectrophotometer Lambda 25 Pelkin Elm).

Results and discussion

Structure analysis of yttrium doped cobalt ferrite was characterized using XRD and FTIR. Meanwhile, the characterization results are displayed in **Figures 1** and **3**. Diffractogram **Figure 1** shows the XRD profile of the powder of cobalt ferrite doped with yttrium at various annealing temperatures. From **Figure 1** of the XRD profile, in all annealing temperatures, observed cobalt ferrite phase in accordance with ICDD data no.221086, which has a face-centred cubic (fcc) structure crystal and Fd-3m space group. Crystallite size can be determined using Scherrer's equation [32].

$$D = \frac{K\lambda}{\beta cos\theta}$$

where K is known as the Scherrer's constant that depends on the geometry of nanoparticles, θ is the profile diffraction angle, β is the full width at half maximum (FWHM) variable at maximum intensity diffraction peak, and λ is the wavelength of the X-ray with Cu-Kα anode.

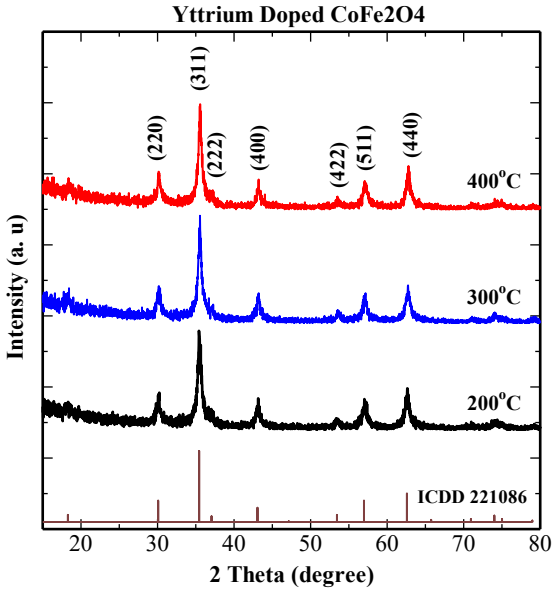

Figure 1 XRD profile of the $CoY_{0.1}Fe_{1.9}O_4$ nanopowder with various annealing temperatures.

The calculation results of the *D* using the Scherrer equation on the highest peak curve of the hkl plane (311) are shown in **Table 1**. The *D* of the $CoY_{0.1}Fe_{1.9}O_4$ nanopowder was obtained at 15.11, 15.33 and 16.05 nm for sintering temperatures of 200, 300 and 400 °C. The findings are a result of a rise in thermal energy within the crystal structure, which also acquaints atomic diffusion and the crystalline groups' growth [33,34]. This rise in the *D* due to increased annealing temperatures aligns with previous research reports [29]. The lattice parameter (*a*) was computed using equation [35].

$$a = d\sqrt{h^2 + k^2 + l^2}$$

where the *d* is the distance between hkl fields.

The substitution of Y elements in the $CoFe_2O_4$ compound leads some of the iron cations (Fe^{3+}) in the octahedral lattice sites to be replaced by yttrium cations (Y^{3+}). Partial replacement of Fe^{3+} cations by Y^{3+} cations causes the change of several inverse spinel lattices to become spinel lattices and causes the lattice constant to decrease slightly. The lattice constant decreases because the octahedral sites on the spinel lattice have a larger radius than the tetrahedral sites. The radius of the Y^{3+} cations can fit snugly at the octahedral lattice sites. Changes in the position of cations between the octahedral and tetrahedral lattice sites can replace small amounts of Fe^{3+} cations with Y^{3+} cations that enter the octahedral sites and reduce the system's energy. The displacement of some Co^{2+} cations from the octahedral to the tetrahedral lattice sites, together with the opposite migration of an equivalent number of Fe^{3+} cations from the tetrahedral sites to the octahedral sites, can reduce energy loss on the octahedral sites. When the annealing temperature increases, some Y^{3+} cations replace Fe^{3+} cations at the octahedral lattice in the cobalt ferrite compound. In the spinel lattice, the octahedral lattice site has a larger radius than the tetrahedral lattice site (A), so that Y^{3+} cations can enter the octahedral sites (B). Simultaneously with the movement of Fe^{3+} cations to the tetrahedral sites, a number of Co^{2+} ions were transferred from the tetrahedral lattice sites to the octahedral lattice sites. Relocation of cations between octahedral and tetrahedral sites can lead to a lower value in the lattice constant as the annealing temperature increases [19].

Furthermore, the low synthesis temperature (200, 300 and 400 °C) produces a decrease in the *a*, i.e., 8.372, 8.384 and 8.391 Å, respectively (**Table 1**). The *a* is increasing in length due to the addition of thermal vibrations of the yttrium-doped element atoms to the surrounding atoms and the increase in annealing temperatures. The crystallite size *D* rises as the annealing temperature is raised, which reduces the $CoY_{0.1}Fe_{1.9}O_4$ nanopowder's specific surface area (*SSA*).

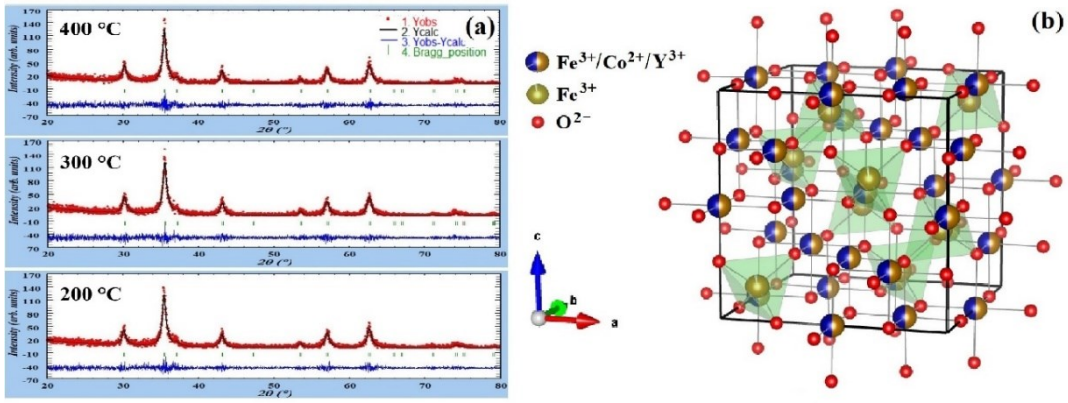

Figure 2 (a) Rietveld refinement of the $CoY_{0.1}Fe_{1.9}O_4$ nanopowder with various annealing temperatures; (b) Representative results of the crystal structure refinement by Rietveld using the Vesta software.

Figure 2(a) shows the results of the refinement of the Rietveld method through Fullprof software from yttrium-doped cobalt ferrite samples at different sintering temperatures. The red dot is the intensity of the observation data from the XRD scanning, the black line is the intensity of the model created through Fullprof software, and the blue line is the difference between the intensity of the observation data and the intensity of the model data carried out by the refinement process. **Figure 2(b)** shows the molecular structure model of the cobalt ferrite compound doped with yttrium based on the refinement results.

Table 1 Crystalline parameters of the $CoY_{0.1}Fe_{1.9}O_4$ nanopowder.

Crystal parameter	**$CoY_{0.1}Fe_{1.9}O_4$**		
	200 °C	**300 °C**	**400 °C**
Crystal system	Cubic	Cubic	Cubic
Space group	Fd-3m	Fd-3m	Fd-3m
R_{Bragg}	7.438	8.681	11.91
R_p	4.921	7.339	10.92
χ^2 (Good of fitness)	1.162	1.130	1.121
Lattice parameter ($a = b = c$) (Å)	8.371776	8.384282	8.390989
$\alpha = \beta = \gamma$	90.0 °	90.0 °	90.0 °
Volume unit (Å^3)	586.81	588.38	590.81
Crystallite size (D) (nm)	15.11	15.33	16.05
Microstrain (ε) ($\times 10^{-3}$)	1.65	2.25	1.14
Density (ρ) (g/cm^3)	5.341	5.354	5.378
Specific surface area (SSA) (m^2/g)	74.34	73.10	69.51

Figure 3 denotes the FTIR pattern of the $CoY_{0.1}Fe_{1.9}O_4$ nanopowder with different annealing temperature variations. Each material has a distinctive infrared absorption spectrum pattern, and the absorption spectrum is useful for determining and identifying the emergence of functional groups present in the material [35]. The inset image presents an enlarged FTIR curve around a typical absorption peak. The inset image shows that the absorption properties only appear around the wavenumber of 582 cm^{-1} for Fe - O bonding and 385 cm^{-1} for Co - O bonding. The characteristics of this FTIR curve indicate the presence of a typical metal-oxygen bond owing to the cobalt ferrite-based nanoparticle magnetic. Changes in the annealing temperature treatment did not significantly affect the shift in the absorption peak on the functional groups of metal-oxygen bonds (M-O), namely the bonding of Cobalt atoms with Oxygen and Iron with Oxygen. Additionally, the emergence of Y^{3+} ions, which take the place of Fe^{3+} ions in the

$CoY_{0.1}Fe_{1.9}O_4$ nanopowder, can be linked to this shift. Small peaks at absorption wave numbers 1,383 and 1,629 cm^{-1} are related to a small number of impurity functional groups, such as compounds of NO_3^{-2} as symmetric vibration and H_2O as bending vibration at absorption [30].

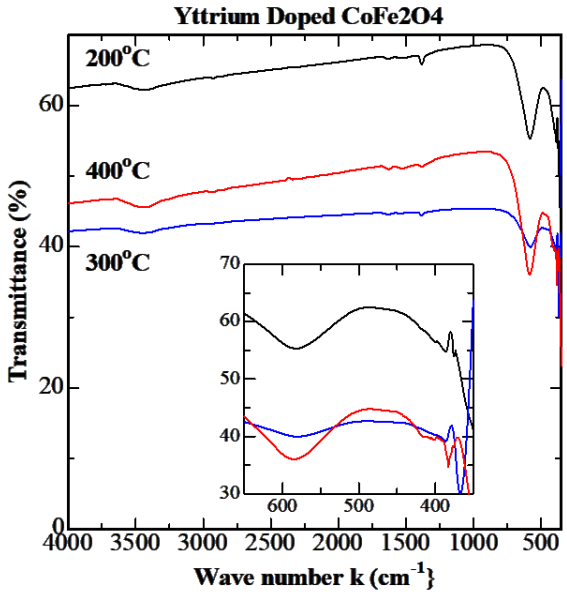

Figure 3 The FTIR curve of the $CoY_{0.1}Fe_{1.9}O_4$ nanopowder at various annealing temperatures.

The force constant octahedral (k_o) and tetrahedral (k_t) sites from FTIR data at the various annealing temperatures are summarized in **Table 2**. The iron-oxygen bonding has an average wave number of 582.21 cm^{-1}, and the cobalt-oxygen bonding has an average wave number of 385.46 cm^{-1}. The averages of the k_t and the k_o are 251.43 and 108.92 N/m, with an average force magnitude (F) of around 180.17 N/m, which indicates the magnitude of the bonding force on M-O.

Table 2 The force constant of metal-oxygen bonding.

Annealing temperature	Fe-O (cm^{-1})	Co-O (cm^{-1})	k_t (N/m)	k_o (N/m)	F (N/m)
200 °C	581.56	386.74	250.87	109.65	180.26
300 °C	580.60	386.74	250.04	109.65	179.84
400 °C	584.46	382.89	253.37	107.47	180.42

Figure 4 shows the magnetization measurement of the $CoY_{0.1}Fe_{1.9}O_4$ nanopowder at various annealing temperatures. It is looked that the saturation magnetization reduces with the rising of the annealing temperature respectively, i.e., 36.84, 34.85 and 30.79 emu/g. The infiltration of yttrium atoms caused this decrease in magnetic saturation into the $CoFe_2O_4$ compound, replacing the position of the Fe atom when the sintering temperature is increased. On the contrary, the coercive field increases with increasing sintering temperature. The calculation of the magnetic parameters, including the saturation magnetization (M_S), coercive field (H_C), total magnetic moment (n_B), remanent magnetization (M_R), and magnetic anisotropy constant (K_a), was summarized in **Table 3**. The reduction in the M_S can be characterized by the redistribution of Co^{2+} ions migration to the tetrahedral site with increasing sintering temperature. The redistributed Co^{2+} ions, due to the annealing temperature, occupy the available tetrahedral vacancies instead of Fe^{3+} ions. Another reason for migration is the increasing influx of Y^{3+} ions, which replace Fe^{3+} ions at octahedral sites. Instead of pushing Co^{2+} ions to migrate, increasing the annealing temperature can decrease the M_S. This result is also supported by the calculation results for the n_B, which decrease with increasing annealing temperature [36].

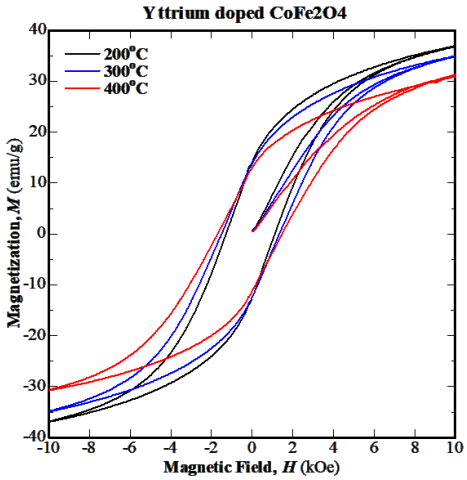

Figure 4 The VSM curve of the $CoY_{0.1}Fe_{1.9}O_4$ nanopowder at various annealing temperatures.

Meanwhile, the H_C of 1,206 Oe for temperature annealing of 200 °C increases to 1,426 and 1,588 Oe for 300 and 400 °C, respectively. Here, the domain wall pinning in the interface is attributed to the increase of the H_C. The availability of the yttrium cation is another factor in the relatively high H_C for cobalt ferrite-based nanoparticle magnetic.

The magnetization close to the saturation could be stated as [36];

$$M = M_S\left(1 - \frac{b}{H^2}\right) + K_a H$$

where $b = \frac{8}{105}\frac{K_1^2}{\mu_0^2 {M_S}^2}$

where the M is the magnetization, the μ_o is the permeability variable of the free space, the H is the applied magnetic field, the K_a is the magnetic anisotropy constant, the K_1 is the cubic anisotropy constant variable, and the term K_1H is known as the forced magnetization variable.

Table 3 The magnetization saturation (Ms), total magnetic moment (nB), remanent magnetization (Mr), and magnetic anisotropy constant (K_a) for various annealing temperatures.

Annealing temperature	H_C (Oe)	M_S (emu/g)	M_R (emu/g)	n_B (μB)	K_1(x10^5) (erg/cm^3)
200 °C	1,206	36.84	13.26	1.55	4.63
300 °C	1,426	34.85	13.21	1.46	5.18
400 °C	1,588	30.79	12.05	1.29	5.09

The morphology of the $CoY_{0.1}Fe_{1.9}O_4$ nanopowder is presented in **Figure 5(a)**. The surface of the $CoY_{0.1}Fe_{1.9}O_4$ nanopowder was viewed using SEM at 150,000 times magnification. **Figure 5(a)** shows the nanopowder of $CoY_{0.1}Fe_{1.9}O_4$ sample observed on a sub-micrometer or nanometer scale.

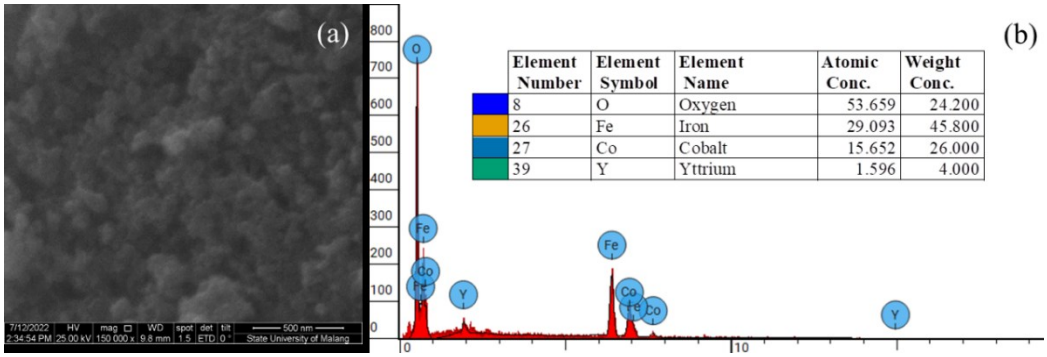

Figure 5 (a) The SEM images and (b) EDX spectra of the $CoY_{0.1}Fe_{1.9}O_4$ nanopowder.

Figure 5(b) shows the EDX results confirm the amount stoichiometry of the $CoY_{0.1}Fe_{1.9}O_4$ nanopowder product. The ratio Y: Co the cobalt ferrite nanopowder of 10.1 % (=1.596/15.652*100 %) is obtained in the experiment using the synthesis method of sol-gel auto-combustion.

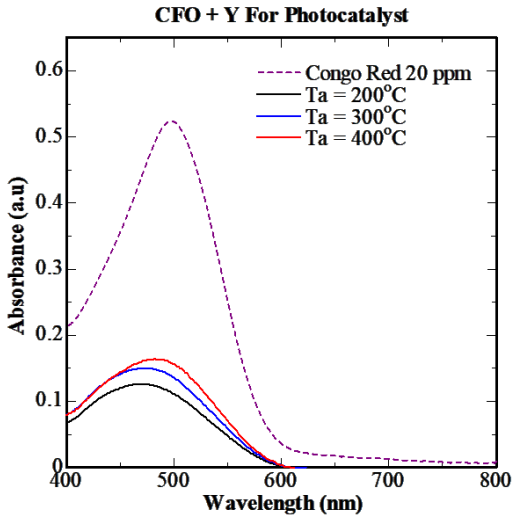

Figure 6 The photocatalytic performance of the $CoY_{0.1}Fe_{1.9}O_4$ nanopowder for various annealing temperatures.

Figure 6 shows the UV-Vis curve resulting from the photocatalytic degradation of $CoY_{0.1}Fe_{1.9}O_4$ nanopowder at various annealing temperatures. The semiconductor $CoFe_2O_4$ oxide, which is doped with yttrium, can have the ability to decompose the Congo Red coloring compound into other compounds that are harmless under 30-min UV irradiation. UV radiation functions as a photocatalyst to decompose dye compounds into other harmless substances. The performance of the 20 mg $CoY_{0.1}Fe_{1.9}O_4$ nanopowder absorbing or decomposing the 20 ppm Congo Red (CR) dye compound via a photocatalyst can be seen in **Table 4** and **Figure 6**. In this experiment, the CR compound was dissolved in 20 ppm of distilled water.

Table 4 The performance of photocatalytic yttrium doped cobalt ferrite ($CoY_{0.1}Fe_{1.9}O_4$) for synthesis sintering temperatures of 200, 300 and 400 °C.

Annealing temperature	C_0	C	Efficiency (%)
200 °C	0.523	0.125	76.10
300 °C	0.523	0.150	71.32
400 °C	0.523	0.168	67.88

The photocatalyst degradation percentage can be calculated using the following equation [37];

$$Efficiency\ (\%) = \frac{C_0 - C}{C_0} \times 100\%$$

C_0 is absorbance before ultraviolet (UV) irradiation, and C is absorbance after UV irradiation with increasing temperatures. UV irradiation is a function of photocatalysis. **Table 4** shows that the yield of photocatalyst degradation decreases with increasing annealing temperature, i.e., 76.10, 71.32 and 67.88 % at 200, 300 and 400 °C, respectively. The decrease that occurs is associated with a decrease in surface area due to an increase in crystallite or particle size; the smaller the size of the nanoparticles, the greater the contact with the test material [38]. The best CR degradation performance results were obtained by the $CoY_{0.1}Fe_{1.9}O_4$ nanopowder at 200 °C, namely 76.10 %, with a *D* of 15.11 nm and an *SSA* of 74.34 m^2/g. These results prove that yttrium-doped cobalt ferrite has opportunities in developing photocatalyst applications.

Conclusions

Yttrium-doped cobalt ferrite nanoparticles with the chemical formula $CoY_{0.1}Fe_{1.9}O_4$ have been successfully synthesized by the sol-gel auto-combustion method. The obtained sample was annealed at the atmospheric conditions with temperatures of 200, 300 and 400 °C for 4 h. The XRD results show that the final samples of the yttrium doped cobalt ferrite sample are owed a single phase of spinel with a space group of Fd-3m. From the Scherrer equation calculation, the crystalline size D increases with the increase in annealing temperature, namely 15.11, 15.33 and 16.05 nm. Fourier-transform infrared (FTIR) spectroscopy results showed the presence of metal-O bonds around the wavenumbers (k) 385 and 582 cm^{-1}, a characteristic of cobalt ferrite compounds. From the VSM measurement, it can be seen that there is a decrease in magnetic saturation with the increase in annealing temperature, i.e., 36.84, 34.85 and 30.79 emu/g. Here, the Yttrium non-magnetic cation replaces the Fe cation, decreasing the total magnetic moment nanoparticle magnetic sample appearance as the reduced magnetization saturation. Finally, the availability of the yttrium cation is another factor in the relatively high Hc for cobalt ferrite-based nanoparticle magnetic. From Scanning Electron Microscopy (SEM), images showed samples have nanoparticle crystallite sizes that have future prospective as pollutant absorbent material. The best photocatalytic degradation results in Congo Red dye were obtained from $CoY_{0.1}Fe_{1.9}O_4$ at 200 °C at 76.10 %. These results indicate that yttrium doped with cobalt ferrite has the potential for photocatalyst applications.

Acknowledgements

This research was funded by RKAT PTNBH of Universitas Sebelas Maret of the Republic of Indonesia through Hibah PDD-UNS with Contract No. 254/UN27.22/PT.01.03/2022.

References

[1] KM Srinivasamurthy, VJ Angadi, SP Kubrin, S Matteppanavar, DA Sarychev, PM Kumar, HW Azale and B Rudraswamy. Tuning of ferrimagnetic nature and hyperfine interaction of Ni^{2+} doped cobalt ferrite nanoparticles for power transformer applications. *Ceram. Int.* 2018; **44**, 9194-203.

[2] PD Prasad and J Hemalatha. Enhanced magnetic properties of highly crystalline cobalt ferrite fibres and their application as gas sensors. *J. Magn. Magn. Mater.* 2019; **484**, 225-33.

[3] S Joshi, VB Kamble, M Kumar, AM Umarji and G Srivastava. Nickel substitution induced effects on gas sensing properties of cobalt ferrite nanoparticles. *J. Alloy. Comp.* 2016; **654**, 460-6.

[4] N Gill, AL Sharma, V Gupta, M Tomar, OP Pandey and DP Singh. Enhanced microwave absorption and suppressed reflection of polypyrrole-cobalt ferrite-graphene nanocomposite in X-band. *J. Alloy. Comp.* 2019; **797**, 1190-7.

[5] MD Ali, A Aslam, T Zeeshan, R Mubaraka, SA Bukhari, M Shoaib, M Amami, I ben Farhat, S ben Ahmed, J Abdelhak and S Waseem. Robust effectiveness behavior of synthesized cobalt doped Prussian blue graphene oxide ferrite against EMI shielding. *Inorg. Chem. Comm.* 2022; **137**, 109204.

[6] VS Kumbhar, AD Jagadale, NM Shinde and CD Lokhande. Chemical synthesis of spinel cobalt ferrite ($CoFe_2O_4$) nano-flakes for supercapacitor application. *Appl. Surf. Sci.* 2012; **259**, 39-43.

[7] M Ghanbari, F Davar and AE Shalan. Effect of rosemary extract on the microstructure, phase evolution, and magnetic behavior of cobalt ferrite nanoparticles and its application on anti-cancer drug delivery. *Ceram. Int.* 2021; **47**, 9409-17.

[8] Z Shi, Y Zeng, X Chen, F Zhou, L Zheng, G Wang, J Gao, Y Ma, L Zheng, B Fu and R Yu. Mesoporous superparamagnetic cobalt ferrite nanoclusters: Synthesis, characterization and application in drug delivery. *J. Magn. Magn. Mater.* 2020; **498**, 166222.
[9] Y Zhang, H Fang, Y Zhang, M Wen, D Wu and Q Wu. Active cobalt induced high catalytic performances of cobalt ferrite nanobrushes for the reduction of p-nitrophenol. *J. Colloid Interface Sci.* 2019; **535**, 499-504.
[10] Y Wang and X Liu. Enhanced catalytic performance of cobalt ferrite by a facile reductive treatment for H2 release from ammonia borane. *J. Mol. Liq.* 2021; **343**, 117697.
[11] B Purnama, AT Wijayanta and Suharyana. Effect of calcination temperature on structural and magnetic properties in cobalt ferrite nano particles. *J. King Saud Univ. Sci.* 2019; **31**, 956-60.
[12] M Hashim, A Ahmed, SA Ali, SE Shirsath, MM Ismail, R Kumar, S Kumar, SS Meena and D Ravinder. Structural, optical, elastic and magnetic properties of Ce and Dy doped cobalt ferrites. *J. Alloy. Comp.* 2020; **834**, 155089.
[13] X Wu, Z Ding, N Song, L Li and W Wang. Effect of the rare-earth substitution on the structural, magnetic and adsorption properties in cobalt ferrite nanoparticles. *Ceram. Int.* 2016; **42**, 4246-55.
[14] G Kumar, RK Singh, SS Kumar, A Manash, A Prabha, U Shankar and O Priya. Low temperature synthesis and influence of Ce^{3+} substitution on structural and magnetic properties of nanocrystalline cobalt ferrite using citrate precursor sol-gel method. *Mater. Today Proc.* 2022; **49**, 1664-9, 2022.
[15] SG Kakade, RC Kambale, YD Kolekar and CV Ramana. Dielectric, electrical transport and magnetic properties of Er3+substituted nanocrystalline cobalt ferrite. *J. Phys. Chem. Solid.* 2016; **98**, 20-7.
[16] A Tijerina-Rosa, JM Greneche, AF Fuentes, J Rodriguez-Hernandez, JL Menéndez, FJ Rodríguez-González and SM Montemayor. Partial substitution of cobalt by rare-earths (Gd or Sm) in cobalt ferrite: Effect on its microstructure and magnetic properties. *Ceram. Int.* 2019; **45**, 22920-9.
[17] M Kamran and M Anis-ur-Rehman. Enhanced transport properties in Ce doped cobalt ferrites nanoparticles for resistive RAM applications. *J. Alloy. Comp.* 2020; **822**, 153583.
[18] M Dhiman and S Singhal. Enhanced catalytic properties of rare-earth substituted cobalt ferrites fabricated by sol-gel auto-combustion route. *Mater. Today Proc.* 2019; **14**, 435-44.
[19] SB Das, RK Singh, V Kumar, N Kumar, P Singh and NK Naik. Structural, magnetic, optical and ferroelectric properties of Y^{3+} substituted cobalt ferrite nanomaterials prepared by a cost-effective sol-gel route. *Mater. Sci. Semicond. Proc.* 2022; **145**, 106632.
[20] DM Ghone, KK Patankar, VL Mathe and SD Kaushik. Influence of substitution of yttrium in cobalt ferrite on the structural, magnetic and magnetostrictive properties. *AIP Conf. Proc.* 2018; **1942**, 130026.
[21] DM Ghone, VL Mathe, KK Patankar and SD Kaushik. Magnetic and magnetostrictive properties of sol-gel prepared Y substituted cobalt ferrite. *AIP Conf. Proc.* 2019; **2115**, 030503.
[22] SS Satpute, SR Wadgane, K Desai, DR Mane and RH Kadam. Substitution effect of Y^{3+} ions on the structural, magnetic and electrical properties of cobalt ferrite nanoparticles. *Cerâmica* 2020; **66**, 43-9.
[23] IH Dunn, SE Jacobo and PG Bercoff. Structural and magnetic influence of yttrium-for-iron substitution in cobalt ferrite. *J. Alloy. Comp.* 2017; **691**, 130-7.
[24] TEP Alves, HVS Pessoni and AF Jr. The effect of Y^{3+} substitution on the structural, optical band-gap, and magnetic properties of cobalt ferrite nanoparticles. *Phys. Chem. Chem. Phys.* 2017; **19**, 16395-405.
[25] A Franco, HVS Pessoni and TEP Alves. Enhanced dielectric permittivity on yttrium doped cobalt ferrite nanoparticles. *Mater. Lett.* 2017; **208**, 115-7.
[26] MK Shobana, W Nam and H Choe. Yttrium-doped cobalt nanoferrites prepared by sol-gel combustion method and its characterization. *J. Nanoscience Nanotechnology* 2013; **13**, 3535-8.
[27] M Ishaque, MA Khan, I Ali, HM Khan, MA Iqbal, MU Islam and MF Warsi. Study on the electromagnetic behavior evaluation of Y^{3+} doped cobalt nanocrystals synthesized via co-precipitation route. *J. Magn. Magn. Mater.* 2014; **372**, 68-73.
[28] M Houshiar, F Zebhi, ZJ Razi, A Alidoust and Z Askari. Synthesis of cobalt ferrite ($CoFe_2O_4$) nanoparticles using combustion, coprecipitation, and precipitation methods: A comparison study of size, structural, and magnetic properties. *J. Magn. Magn. Mater.* 2014; **371**, 43-8.
[29] MK Shobana, H Kwon and H Choe. Structural studies on the yttrium-doped cobalt ferrite powders synthesized by sol-gel combustion method. *J. Magn. Magn. Mater.* 2012; **324**, 2245-8.
[30] X Wu, H Yu and H Dong. Enhanced infrared radiation properties of $CoFe_2O_4$ by doping with Y^{3+} via sol-gel auto-combustion. *Ceram. Int.* 2014; **40**, 12883-9.

[31] MSA Maashani, KA Khalaf, AM Gismelseed and IA Al-Omari. The structural and magnetic properties of the nano-$CoFe_2O_4$ ferrite prepared by sol-gel auto-combustion technique. *J. Alloy. Comp.* 2020; **817**, 152786.
[32] L Kumar, P Kumar, A Narayan and M Kar. Rietveld analysis of XRD patterns of different sizes of nanocrystalline cobalt ferrite. *Int. Nano Lett.* 2013; **3**, 8.
[33] LE Caldeira, CS Erhardt, FR Mariosi, J Venturini, RYS Zampiva, ORK Montedo, S Arcaro, CP Bergmann and SR Bragança. Correlation of synthesis parameters to the structural and magnetic properties of spinel cobalt ferrites ($CoFe_2O_4$) - an experimental and statistical study. *J. Magn. Magn. Mater.* 2022; **550**, 169128.
[34] NA Rana, V Kumar and AM Awasthi. Effect of dopant concentration and annealing temperature on electric and magnetic properties of lanthanum substituted $CoFe_2O_4$ nanoparticles for potential use in 5G wireless communication systems. *Ceram. Int.* 2021; **47**, 20669-77.
[35] E Hutamaningtyas, Utari, Suharyana, AT Wijayanta and B Purnama. FTIR and structural properties of co-precipitated cobalt ferrite nano particles. *J. Phys. Conf. Ser.* 2016; **776**, 012023.
[36] NP Prasetya, RI Setiyani, Utari, Kusumandari, Y Iriani, J Safani, A Taufiq, NA Wibowo, Suharno and B Purnama. Cation trivalent tune of crystalline structure and magnetic properties in coprecipitated cobalt ferrite nanoparticles. *Mater. Res. Exp.* 2023; **10**, 036102.
[37] Riyatun, T Kusumaningsih, A Supriyanto, HB Akmal, FM Zulhaina, NP Prasetya and B Purnama. Nanoparticle-preparation-procedure tune of physical, antibacterial, and photocatalyst properties on silver substituted cobalt ferrite. *Results Eng.* 2023; **18**, 101085.
[38] OK Mmelesi, N Masunga, A Kuvarega, TT Nkambule, BB Mamba and KK Kefeni. Cobalt ferrite nanoparticles and nanocomposites: Photocatalytic, antimicrobial activity and toxicity in water treatment. *Mater. Sci. Semicond. Proc.* 2021; **123**, 105523.